SINAI International Scientific Journal (SISJ)
Volume 1, Issue 4, April 2025

Effect of the Calcination Process on the Structural and Optical Properties of (Ba0.8Ca0.1B0.1)(Ti0.9Zr0.1)O3 Glass

*Essam A. Elkelany[1 *], Abd El-razek Mahmoud[2], Zakaria M. Abd El-Fattah[3,4], M. Farouk[3], Moukhtar A. Hassan[3]*

[1] *Basic Science Department, Faculty of Engineering, Sinai University, Al-Arish 45511, Egypt.*
[2] *Ferroelectric & Piezoelectric Lab, Faculty of Science, South Valley University, Qena, 83523, Egypt.*
[3] *Physics Department, Faculty of Science, Al-Azhar University, Nasr City, E-11884 Cairo, Egypt.*
[4] *Physics Department, Faculty of Science, Galala University, New Galala City, Suez, 43511, Egypt.*
**Corresponding author*

Correspondence:

Essam A. Elkelany
essamelkelany88@gmail.com

Citation:

Elkelany, E., Mahmoud, A,. Abd El-Fattah, Z., Farouk, M.. Hassan, M., " Effect of the Calcination Process on the Structural and Optical Properties of (Ba0.8Ca0.1B0.1)(Ti0.9Zr0.1)O3 Glass ", SINAI International Scientific Journal (SISJ), vol.1 issue 4, pp. 5-18, 2025

Received: 16 May 2024

Accepted: 21 July 2024

ABSTRACT

This paper presents the characterization of two$(Ba_{0.8}Ca_{0.1}B_{0.1})(Ti_{0.9}Zr_{0.1})O_3$ glass samples with the composition 40.0BaO+5.0CaO+5.0B_2O_3+45.0TiO_2+5.0ZrO_2 (BBCZT) using various techniques. The two samples were produced through the melting quenching technique with two different methods. XRD analysis showed that both samples are amorphous. The glass network structure was analyzed using FT-IR spectroscopy, which enabled the identification of the functional groups and vibrational modes associated with the chemical bonds within the material. By applying Archimede's principle, the density (ρ) and molar volume (V_m) of the samples were evaluated. It was observed that the density of one of the samples increased (4.089 - 4.260 g/cm^3), which was attributed to the conversion of BO_3 (81.98%) to BO_4 (89.73%) units in the material. Optical spectra were obtained to determine the optical energy gap (E_{opt}) (2.848 eV - 3.028 eV) and Urbach's energy (ΔE) (0.262 eV - 0.247 eV), which were found to vary between the two samples due to differences in their preparation methods. The linear refractive index (n_0), the dielectric constant (ε), the molar refraction (R_m), the molar polarizability (α_m), and the metallization criterion (M) were also calculated to understand the optical characteristics of the two samples.

KEYWORDS: BCZT glass; Calcination process; Structural properties; Optical properties.

1. INTRODUCTION

Glass is an exceptionally versatile material extensively utilized across various industries, including construction, medical equipment and electronic devices [1–4]. Among glass types, oxide glasses are particularly notable for their wide range of industrial applications, driven by their distinctive properties such as mechanical strength, thermal stability, optical clarity, and chemical resistance [3]. A key application area for oxide glasses is optics, where they are used to manufacture lenses, optical fibers, prisms, and mirrors. These glasses exhibit superior optical properties, including high transparency in specific regions of the electromagnetic spectrum, making them ideal for numerous optical uses [1, 3 ,5]. B_2O_3 is widely favored as a glass-former due to its low melting point, thermal stability, transparency, and advantageous optical and mechanical properties. Additionally, B_2O_3 serves as a melting agent in glass manufacturing, enhancing the solubility of other oxides, which reduces the melting temperature and improves the homogeneity of the glass composition [1, 2, 5].

The B_2O_3 glass network comprises two structural units, BO_3 and BO_4, with their ratio influenced by various factors, including the glass composition and the preparation method [4]. TiO_2 possesses several unique characteristics, such as a wide band gap, high refractive index, chemical stability, and photocatalytic activity, making it suitable for diverse applications [6 –

Online ISSN: 3009-7800
Print ISSN: 3009-6324

9], and enhancement of the glass-forming ability through the contribution of TiO_4 and TiO_5 units in the glass network structure as building units [7, 10]. The composition($Ba_{0.85}Ca_{0.15}Ti_{0.9}Zr_{0.1}$) (BCZT) is recognized as a lead-free ferroelectric ceramic material with significant potential for electronic applications, including piezoelectric and pyroelectric devices, capacitors, actuators, transducers, and energy harvesting and storage systems. BCZT's importance in the electronics industry stems from its remarkable properties, such as a high piezoelectric coefficient (d_{33}), dielectric constant (ε), electromechanical coupling factor (kp), and environmentally friendly nature. However, producing pure perovskite-phase BCZT ceramic requires extremely high temperatures for calcination (up to 1350°C) and sintering (up to 1500°C) [11 - 14].

Several studies have explored the characteristics of BCZT as a ceramic material. Despite its notable ceramic properties, there has been a lack of research investigating BCZT as a glass material. This paper aims to examine the structural and optical properties of BCZT when used as a glass material. Additionally, it explores the impact of the calcination process of oxides before the melting quenching process on the optical and structural properties of the composition. Producing pure BCZT glass requires high temperatures exceeding 1500°C to reach its melting point. To address this challenge, B_2O_3 was added to the BCZT composition, serving as a melting agent. B_2O_3 not only lowers the melting point but also contributes to the formation of the glass network structure.

2. EXPERIMENTAL SECTION

Two glass samples with the same composition $(Ba_{0.8}Ca_{0.1}B_{0.1})(Ti_{0.9}Zr_{0.1})O_3$ were produced through the melting quenching technique with two different methods. The glass samples were named BBCZT1 and BBCZT2 glasses. $BaCO_3$, $CaCO_3$, ZrO_2, TiO_2, and BH_3O_3 were used as precursor materials. The first sample (BBCZT1), was papered by weighing the raw materials according to the specified proportions, and then the materials were blended and pulverized using an agate mortar.

The resulting mixture was then transferred to a porcelain crucible and subjected to a temperature of 1450°C in an electric oven for 1 h. In the second sample (BBCZT2), the $(Ba_{0.8}Ca_{0.1}B_{0.1})(Ti_{0.9}Zr_{0.1})O_3$ composition was papered as a calcined powder. The $(Ba_{0.8}Ca_{0.1}B_{0.1})(Ti_{0.9}Zr_{0.1})O_3$ calcined powder was synthesized using BH_3O_3, $BaCO_3$, $CaCO_3$, ZrO_2 and TiO_2 as precursor materials. The materials were weighed and mixed using a ball milling (E max 5ACC2, Germany) in ethanol with zirconia balls media for 24 h. The mixed materials were dried and then calcined at 1300°C for 2h in the air. Second, the BBCZT calcined powder was ground with an agate mortar to obtain the fine powder and placed in a porcelain crucible and put in an electric oven for 1h at a temperature of 1450°C. To ensure that the molten substances had a uniform composition, they were thoroughly mixed by swirling during the melting process. Finally, the melts were subjected to a fast cooling process to bring them to room temperature (RT). The amorphous nature of the BBCZT glass samples was examined by X-ray diffraction (Bruker D8 Advance) with Cu kα radiation (λ=1.5406 Å) at 40 mA, 40kVand RT in the 2θ range (20-80). Archimedes's principle was employed to calculate the density of the samples at RT using distilled water as an immersion liquid. Fourier-transform infrared (FT-IR) measurement was performed at RT using the Thermo FT-IR 200 spectrometer. Optical measurement was carried out at RT by the JASCO V-670 UV–Vis spectrophotometer.

Online ISSN: 3009-7800
Print ISSN: 3009-6324

3. RESULTS AND DISCUSSION

3.1. XRD Measurement

The XRD spectra of the two glass samples, as illustrated in Fig. 1, do not display any distinct peaks. The absence of sharp peaks emphasizes the amorphous nature of the samples [2, 15].

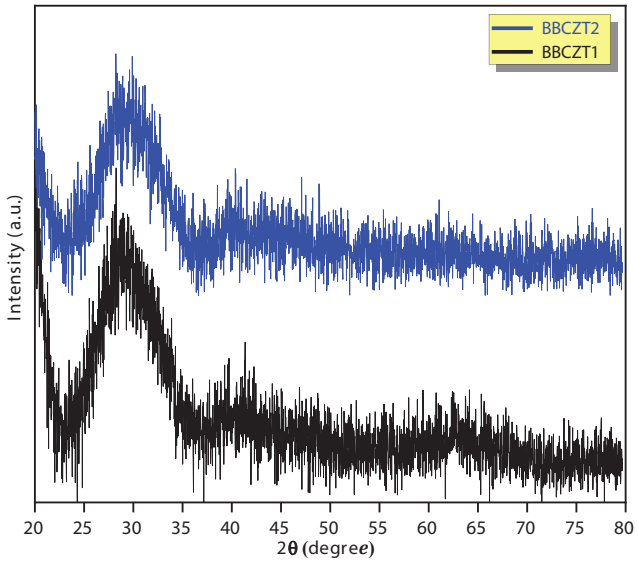

Fig. 1: XRD of the BBCZT glass samples

3.2. Infrared Spectra (IR)

The two glass samples were examined using an FT-IR spectrometer to specify the functional groups and vibrational modes associated with the chemical bonds within the network structure of the glass.

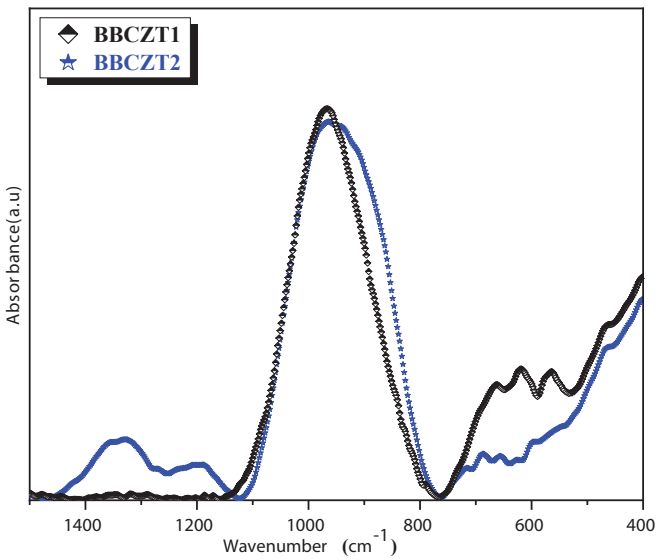

Fig. 2: FTIR spectra for the BBCZT glass samples

Online ISSN: 3009-7800
Print ISSN: 3009-6324

Fig. 2 shows the FT-IR spectra of the glass samples, encompassing the range of 400 - 1600 cm^{-1}. The FT-IR spectrum of BBCZT1 has a band in the range of 1100 - 1500 cm^{-1}. This band disappears in BBCZT2 FT-IR spectra. The FT-IR spectra were subjected to a deconvolution process using the Gaussian function to remove the overlap between the peaks and determine the exact peak positions, as illustrated in Fig. 3.

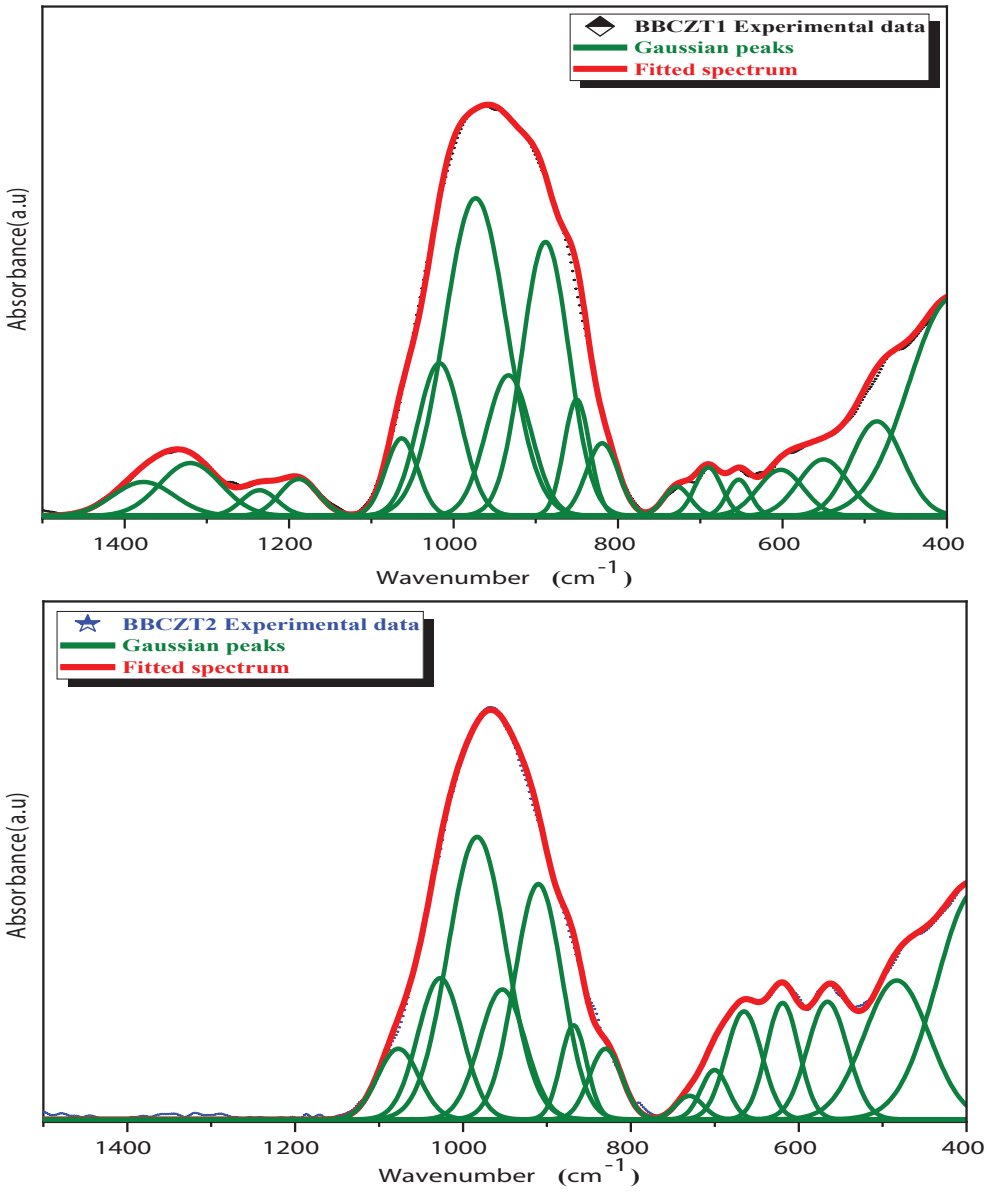

Fig. 3: Deconvolution process for FTIR spectrum for the BBCZT glass samples

The deconvolution process produced seventeen peaks for BBCZT1 spectra and fourteen peaks for BBCZT2 spectra. Table 1 provides the peak position (Xc), area (A), full width at half maximum (W), and corresponding peak assignments. Disappearing The band in the region of 1100 - 1500 cm^{-1} in the BBCZT2 FT-IR spectra and the increasing band in the region of 800 - 1200 cm^{-1} resulted from the transformation of BO_3 units to BO_4 units (i.e., conversion of the network structure from opened to closed structure) [1, 4].

Online ISSN: 3009-7800
Print ISSN: 3009-6324

Table. 1: Centers and assignments of Peaks in the FT-IR absorption spectra of BBCZT1 and BBCZT2 samples.

Peak No	BBCZT1			BBCZT2			Assignment (vibration modes of the bonds in the structural units)
	X_C cm^{-1}	W cm^{-1}	A a.u.	X_C cm^{-1}	W cm^{-1}	A a.u.	
1	~400	150	0.680	~400	130	0.635	vibration of Ca^{2+} metal cation[16,17].
2	485	89	0.437	483	110	0.817	vibration of Zr-O bond in ZrO_6 unit[18–20].
3	550	85	0.249	565.5	68	0.428	vibration of Ba^{2+} metal cation as well as TiO_4 units [21–23].
4	602	78	0.187	619	55	0.343	B–O–B bending vibration in BO_3 as well as deformation modes of borate rings[4,16,24].
5	653	40	0.076	665	60	0.347	Ti–O symmetric stretching vib in Ti-O-Ti bridge connected with TiO6[23,25–27].
6	690	46	0.116	700	46	0.122	B–O–B symmetric bending vibration in BO_3 [1,4,28].
7	728	46	0.069	730	46	0.058	stretching vibration of Ti-O bonds in TiO_5 [29,30].
8	819	55	0.208	830	55	0.208	Vibration of the oxygen bridge atoms connecting a tetrahedral structure with a trigonal boron group[25].
9	850	44	0.266	868	44	0.221	tensile vibration of Ti–O-Ti in TiO_4[27].
10	888	80	1.138	910	80	1.007	NBOs in BO_4 unit[4,24].
11	933	77	0.562	953	77	0.535	B–O rocking and stretching vibrations in BO_4[4,24,31,32].
12	973	106	1.747	983	98	1.480	B–O rocking and stretching vibrations in BO_4[4,24,31,32].
13	1017	75	0.595	1027	75	0.566	B–O rocking and stretching vibrations in BO_4[4,24,32,33].
14	1063	55	0.221	1077	70	0.264	B–O rocking and stretching vibrations in BO_4[4,24,32,33].
15	1188	66	0.126	-	-	-	B–O asymmetric stretching of (NBOs) in BO_3[4,24,32].
16	1236	61	0.081	-	-	-	B–O asymmetric stretching in BO_3[4,24,32,33].
17	1320	105	0.288	-	-	-	B–O asymmetric stretching in BO_3[4,24,32,33].
18	1377	105	0.185	-	-	-	B–O asymmetric stretching in BO_3[4,24,32,33].

The N_4 and N_3 values were determined through the equation [4, 16]:

$$N_4 = A_4 / (A_4 + A_3) \quad (1)$$

$$N_3 = A_3 / (A_4 + A_3) \quad (2)$$

The values of A_4 and A_3 correspond to the peak areas of BO_4 and BO_3, respectively. The ratio of NBOs is determined by the following equation:

$$\text{NBOs} = \frac{\text{NBO}_{BO_4} + \text{NBO}_{BO_3}}{A_4 + A_3} \quad (3)$$

Here, NBO_{BO_4} and NBO_{BO_3} denote the area under the deconvoluted peaks at approximately 905 cm^{-1} in the BO_4 region and 1188 cm^{-1} in the BO_3 region, respectively. The N_4 value increases from 81.98% in BBCZT1 to 89.73% in BBCZT2, while the NBO's

Online ISSN: 3009-7800
Print ISSN: 3009-6324

percentage decreases from 23.17% in BBCZT1 to 22.25% in BBCZT2, as depicted in Fig 4. The observed increase in N_4 coupled with the decrease in NBOs indicates that the calcination process leads to a more uniform glass structure by converting BO_3 to BO_4 units and reducing the presence of NBO's.

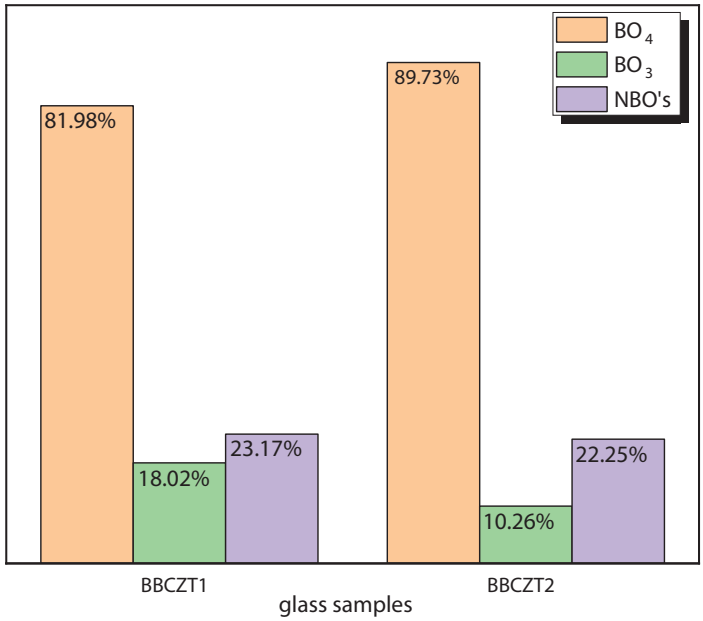

Fig. 4: N4, N3 and NBOs ratios of BBCZT glass samples

3.3. Density (ρ) and Molar Volume (V_m)

The ρ of the samples was estimated based on Archimedes' principle and according to the relation:

$$\rho = \rho_{liquid}\left(\frac{W_{air}}{W_{air} - W_{liquid}}\right) \quad (4)$$

Where ρ_{liquid} is the density of immersion liquid, W_{air} represents the weight of the sample in the air, while W_{liquid} represents the weight of the same sample when it is submerged in liquid [17]. The ρ of BBCZT1 and BBCZT2 are 4.089 and 4.260 g/cm^3, respectively. Increasing the ρ of BBCZT2 is owing to the conversion of BO_3 units with non-bridging oxygen (NBOs) to BO_4 units (i.e., conversion of the network structure from opened to closed structure). The arrangement of atoms and the decrease in voids are due to the calcination process. The V_m of the samples was computed using the equation:

$$\rho = \rho_{liquid}\left(\frac{W_{air}}{W_{air} - W_{liquid}}\right) \quad (5)$$

Where M_T is the overall molecular weight [4, 18]. The V_m of BBCZT1 and BBCZT2 are 49.924 and 47.923 cm^3/mol., respectively. Decreasing the V_m of BBCZT2 than BBCZT1 is owing to an increase in the ρ of BBCZT2 with no change in the M_T of the two samples. The values of the ρ and V_m are listed in Table 2.

Online ISSN: 3009-7800
Print ISSN: 3009-6324

Table.2: Density (ρ), molar volume (V_M), Optical band gap (E_{opt}), Urbach's energy (ΔE), linear refractive index (n_0), dielectric constant (ε), molar refraction (Rm), Molar polarizability (α_m), metallization criterion (M), third-order non-linear optical susceptibility ($\chi^{(3)}$) and non-linear refractive index (n_2) for the glass samples.

Sample code	ρ (g/cm^3)	V_M (cm^3/mol)	E_{opt} (eV)	ΔE (eV)	n_0	ε	R_m (cm^3/mol)	α_m (×10^{-24}cm^3)	M (eV$^{0.5}$)	$\chi^{(3)}$ (×10^{-14}esu)	n_2 (×10^{-12}esu)
BBCZT1	4.089	49.924	2.848	0.262	1.685	2.838	18.967	7.516	0.377	7.774	1.740
BBCZT2	4.260	47.923	3.028	0.247	1.705	2.906	18.614	7.376	0.389	8.976	1.986

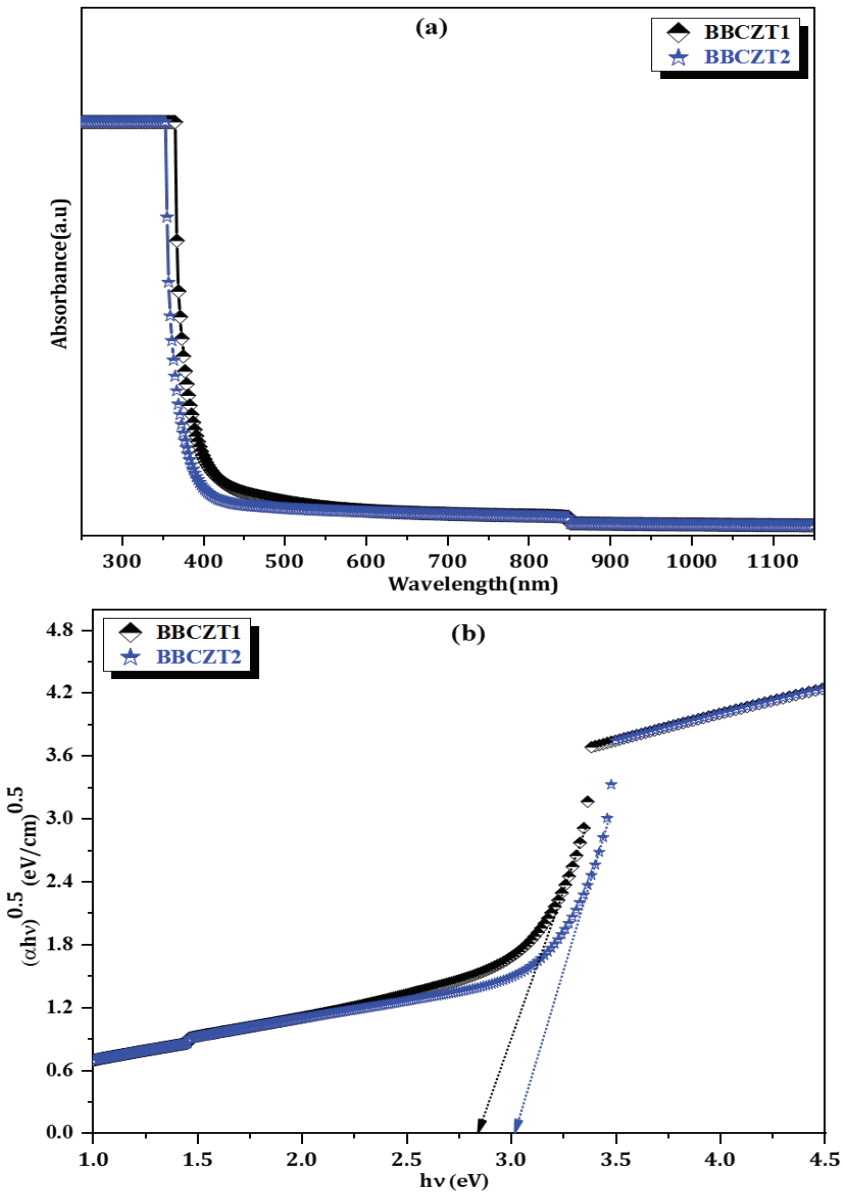

Fig. 5: (a) Optical absorption spectra for the BBCZT glass samples and (b) Tauc's plot for the BBCZT glass samples.

Online ISSN: 3009-7800
Print ISSN: 3009-6324

3.4. Optical Properties

Fig. 5a shows the optical absorption spectra of the two samples. The gradual optical absorption edges of the two samples suggest that the samples have an amorphous structure [4]. The optical energy gap (E_{opt}) and bandwidth of the localized tail states or Urbach's energy (ΔE) were calculated. The E_{opt} is an important factor for understanding the optical and electronic characteristics of the glasses, and it has significant effects on their use in various applications. The E_{opt} in glasses is essential for determining their color, transparency, and various optical properties. ΔE is a significant parameter that reflects the atomic structural disorder in glass. ΔE arises due to the presence of structural disorder, defects, and impurities within the glass [19, 20]. E_{opt} was calculated through the relation [33]:

$$\alpha\ \upsilon = B(\ \upsilon - E_{opt})^{b} \tag{6}$$

Where α is the optical absorption coefficient and can be calculated from the equation[4]:

$$\alpha(\upsilon) = 2.303\,(A/t) \tag{7}$$

Here, A refers to the absorbance of the sample, while t represents its thickness. hυ denotes the energy of the incident photons, and B represents the band tailing parameter. The factor b takes on different values of 1/2, 2/3, 2, or 3 depending on the electronic transition, which can be direct allowed, direct forbidden, indirect allowed, or indirect forbidden transitions, respectively [34]. Factor b was chosen as 2 (indirect allowed) from the different factors, wherein the amorphous materials the most likely type of electronic transitions that occur is the indirect allowed transition [22]. The values of E_{opt} for the samples were estimated by extrapolating the liner portion of $(\alpha h\upsilon)^{1/2}$ against hυ and determining the intersect position with the X axis at $(\alpha h\upsilon)^{1/2}$ equal to zero as illustrated in Fig. 5b [34]. The values of the E_{opt} are listed in Table 2. ΔE was calculated through the relation:

$$\alpha = \alpha_0 \exp\left(\frac{\upsilon}{\Delta E}\right) \tag{8}$$

Where $\alpha_0$is a characteristic parameter depending on the type of material. The values of ΔE were estimated by drawing *ln(α)* against *hυ* and determining the inverse slope of the liner portion (not shown) [23]. The values of ΔE are presented in Table 2. The value of E_{opt} increases from 2.848 eV for BBCZT1 to 3.028 eV for BCZT2 as shown in Fig. 6a. The difference in E_{opt} of the same composition for BBCZT1 and BBCZT2 is attributed to the variation of electronic band structure for the two samples due to the variation of preparation method. Where The BBCZT2 sample was subjected to the calcination process before the melting process. The calcination process promotes the formation of a uniform crystal structure and leads to long-range order for the structure of the sample [24, 25]. The BBCZT2 sample may have retained some of this order during the melting process. So, the atoms in BBCZT2 are more orderly and regular than in BBCZT1. The disorder of BBCZT1 induced localized states inside the band gap, which can trap electrons and decrease the optical energy gap [26, 27]. Moreover, the conversion of BO_3 units with NBOs to BO_4 units leads to an increase in the E_{opt}. Where the electrons in NBOs require less energy to be excited to higher levels than electrons in bridging oxygen's (BOs) [4]. The decrease of ΔE from 0.262 eV for BBCZT1 to 0.247 eV

Online ISSN: 3009-7800
Print ISSN: 3009-6324

for BCZT2 as shown in Fig. 6b is an indication of reducing the number of structural defects, localized states, and enhancement of the structure ordering and stability of the glass network [17, 20, 23].

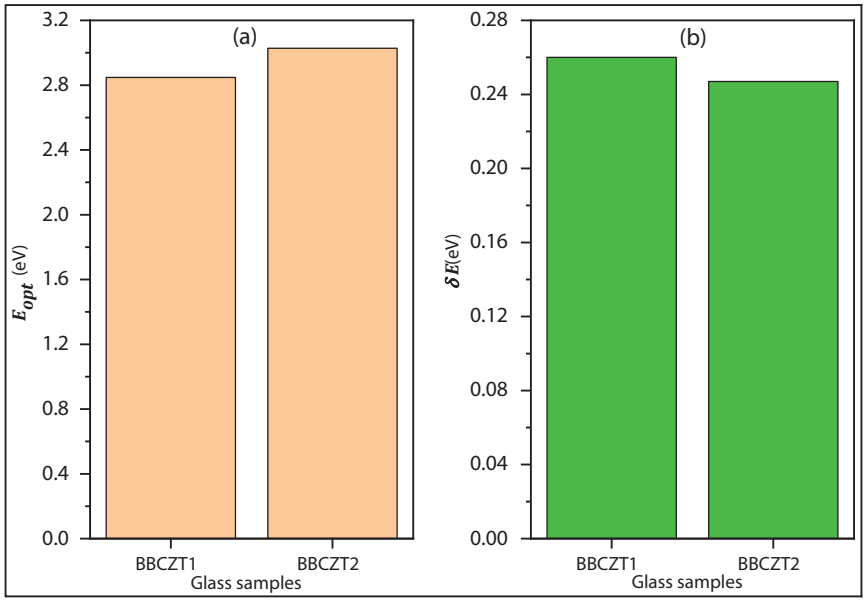

Fig. 6: (a) E_{opt} of BBCZT glass samples and (b) ΔE of BBCZT glass samples

Linear refractive index (n_0), the dielectric constant (ε), the molar refraction (R_m), the molar polarizability (α_m), and the metallization criterion (M) are estimated through the following equations [4, 28, 29]:

$$n_o = \frac{\rho + 10.4}{8.6} \tag{9}$$

$$= n_0^2 \tag{10}$$

$$R_m = \frac{V_m(n_0^2 - 1)}{(n_0^2 + 2)} \tag{11}$$

$$R_m = \frac{4\pi N_A \alpha_m}{3} \tag{12}$$

$$\alpha_m = \frac{3R_m}{4\pi N_A} \tag{13}$$

The linear refractive index (n_0) increases from 1.685 for BBCZT1 to 1.705 for BBCZT2, the increment of the linear refractive index (n_0) can be interpreted in terms of the increase in the density and optical band gap of the BBCZT2 sample. The decrease in polarizability is ascribed to the enhancement in the arrangement of atoms, decrease in defects, and number of NBOs in the glass network [28, 30, 31]. The metallization criterion (M) was calculated through the relation [32, 33] :

Online ISSN: 3009-7800
Print ISSN: 3009-6324

$$M = \sqrt{\frac{E_{opt}}{20}} \tag{14}$$

The metallization criterion (M) provides a valuable means of predicting the conductive properties of a material, distinguishing between metallic, non-metallic, or semimetal behavior. Specifically, M tends to be close to zero for metallic behavior, approaches one for non-metallic behavior, and falls within the range between zero and one for semimetal behavior [32, 33]. The metallization criterion (M) increases from 0.377 for BBCZT1 to 0.389 $eV^{0.5}$ for BBCZT2. The increment in the metallization criterion for BBCZT2 indicates a shift toward non-metallic behavior and is compatible with the decreasing of NBOs ratio. The values of the linear refractive index (n_0), the dielectric constant (ε), the molar refraction (R_m), the molar polarizability (α_m), and the metallization criterion (M) are tabulated in Table 2.

Nonlinear optical properties (NLO) describe how the interaction between light and matter changes as the light's intensity increases. The nonlinearity of a medium can alter the way light interacts with it, affecting the refractive index, absorption, or generating new frequencies [34]. Nonlinear optical effects manifest when light interacts with a nonlinear medium because light does not inherently exhibit nonlinearity. This interaction generates a field within the material that can alter the behavior of the incident light [35]. NLO properties are crucial for various applications, including optical limiters, fiber optics, 3D microfabrication, frequency up-conversions, photorefractive materials, passive mode locking, optical switches and high-speed electro-optic modulators [34, 36]. The non-linear refractive index (n_2) is a measure of the reply of a matter to the intensity of an electromagnetic field, and it changes with the intensity of the field in contrast to the linear refractive (n_0) index. The non-linear refractive index (n_2) can be computed from the relation [29, 37]:

$$n_2 = \frac{12\pi\chi^{(3)}}{n_0} \tag{15}$$

$$\chi^{(3)} = 1.7 \times 10^{-10}\left(\frac{n_0^2 - 1}{4\pi}\right)^4 \tag{16}$$

Where $\chi^{(3)}$ is the 3rd-order non-linear optical susceptibility. The values of $\chi^{(3)}$ and n_0 are recorded in Table 2. The reason why BBCZT1 has a higher value of $\chi^{(3)}$ and n_2 compared to BCZT2 may be due to its lower E_{opt} [29]. This is because materials with lower E_{opt} typically have a greater number of electronic states available for participating in nonlinear optical processes, resulting in larger non-linear optical susceptibilities and non-linear refractive indices.

4. Conclusion

The characterization of two glass samples (BBCZT1 and BBCZT2) was performed using various techniques. XRD analysis emphasized the amorphous character of the two samples. FT-IR analysis confirmed the existence of structural units (TiO_6-TiO_4-TiO_5-BO_3-BO_4) for the two samples and the conversion of the BO_3 to BO_4 units in the BBCZT2 sample. The density and molar volume measurements indicated that BBCZT2 has a higher density

Online ISSN: 3009-7800
Print ISSN: 3009-6324

(4.260 g/cm^3) and a lower molar volume (47.923 cm^3/mol) than BBCZT1which is owing to the conversion of BO_3 to BO_4 units and the rearrangement of atoms during the calcination process. The optical properties of the two samples were also investigated, and it was discovered that the optical energy gap (E_{opt}) and Urbach's energy (ΔE) values varied between the two samples. The optical energy gap (E_{opt}) of BBCZT2 (3.028 eV) was higher than that of BBCZT1 (2.848 eV), which could be attributed to the formation of a more ordered structure of BBCZT2 than BBCZT1 as a result of the calcination process. The decreasing of Urbach's energy (ΔE) for BBCZT2 (0.247 eV) indicated a reduction of the structural defects and localized states. The linear refractive index (n_0) increases from 1.685 for BBCZT1 to 1.705 for BBCZT2. The metallization criterion (M) of BBCZT2 (0.389) was higher than that of BBCZT1 (0.377), indicating a shift towards non-metallic behavior. These findings suggest that incorporating this technology into the glass-ceramic preparation process can minimize the impact of secondary phases and enhance the properties of the ceramic phase.

DECLARATION

The authors used one of the AI technologies to improve the readability of the review.

CONFLICTS OF INTEREST

None

REFERENCES

[1] Abul-magd AA, Basry AAH, Abu SM, Hassan E, Abu-khadra AS. Interplay between structural modifications and optical / luminescence response in Mn-doped alkali borate glasses. Mater Chem Phys [Internet]. 2022;288(April):126381. Available from: https://doi.org/10.1016/j.matchemphys.2022.126381

[2] Abul-magd AA, Morshidy HY. The role of NiO on the structural and optical properties of sodium zinc borate glasses. Opt Mater (Amst) [Internet]. 2020;109(June):110301. Available from: https://doi.org/10.1016/j.optmat.2020.110301

[3] Morshidy HY, Mohamed AR, Abul-magd AA, Hassan MA. Role of high energy Cr^{6+} optical transition induced by rare earth ion (La^{3+}) in compositional-dependent borate glass. 2022;289(April).

[4] Elkelany EA, Hassan MA, Samir A, Abdel-Ghany AM, El-Bahnasawy HH, Farouk M. Optical and Mössbauer spectroscopy of lithium tetraborate glass doped with iron oxide. Opt Mater (Amst) [Internet]. 2021 Feb;112(October 2020):110744. Available from: https://doi.org/10.1016/j.optmat.2020.110744

[5] Morshidy HY, Mohamed AR, Abul-Magd AA, Hassan MA. Ascendancy of Cr^{3+} on Cr^{6+} valence state and its effect on borate glass environment through CdO doping. Mater Chem Phys [Internet]. 2022 Jun;285(January):126128. Available from: https://doi.org/10.1016/j.matchemphys.2022.126128

[6] Dawngliana KMS, Fanai AL, Rai S. Structural and optical studies of Sm^{3+}-doped silica glass along with TiO2 nanoparticles for photonic applications. J Non Cryst Solids. 2023;607(November 2022).

Online ISSN: 3009-7800
Print ISSN: 3009-6324

[7] Kumar A, Saxena VK, Thangavel R, Nandi BK. A dual effect of surface roughness and photocatalysis of crystalline TiO_2-thin film for self-cleaning application on a photovoltaic covering glass. Mater Chem Phys. 2022;289(March).

[8] Tan H, Zhang Y, Li B, Yang H, Hou H, Huang Q. Preparation of TiO2-coated glass flat membrane and its photocatalytic degradation of methylene blue. Ceram Int. 2023;49(11):17236–44.

[9] Fong WL, Bashar K, Baki SO, Karim MKA, Sayyed MI, Mahdi MA, et al. Influence of Bi_2O_3 content on structural, optical and radiation shielding properties of transparent Bi_2O_3-Na_2O-TiO_2-ZnO-TeO_2 glass ceramics. Radiat Phys Chem [Internet]. 2022 Nov;200(March):110289. Available from: https://linkinghub.elsevier.com/retrieve/pii/S0969806X22003322

[10] Deng L, Fu Z, Gao L, Li H, Du Y, Chen H, et al. P_2O_5/ZrO_2/TiO_2 codoped transparent cordierite glass ceramics: Stability, crystallization and light transmittance. Opt Mater (Amst). 2023;138(December 2022).

[11] Bijalwan V, Tofel P, Erhart J, Maca K. The complex evaluation of functional properties of nearly dense BCZT ceramics and their dependence on the grain size. Ceram Int. 2019;45(1):317–26.

[12] Rafiq MA, Zaman TU, Ishfaq HA, Maqbool A, Waqar M, Muhammad QK, et al. Exploring the conduction mechanism of multiferroic SrM–BCZT composite. Ceram Int. 2020;46(2):2489–99.

[13] Wang X, Huan Y, Zhu Y, Zhang P, Yang W, Li P, et al. Defect engineering of BCZT-based piezoelectric ceramics with high piezoelectric properties. J Adv Ceram [Internet]. 2022 Jan 24;11(1):184–95. Available from: https://link.springer.com/10.1007/s40145-021-0526-6

[14] Lai Y, Zeng Y, Tang X, Zhang H, Han J, Huang Z, et al. Effects of CaO–B_2O_3–SiO_2 glass additive on the microstructure and electrical properties of BCZT lead-free ceramic. Ceram Int. 2016 Aug 15;42(11):12694–700.

[15] Wang Z, Xu R. Non-isothermal crystallization kinetics of CaO-SiO_2-B_2O_3-TiO_2 glass studied by differential thermal analysis in the case of “site saturation.” Ceram Int [Internet]. 2023 Jun;49(11):19346–54. Available from: https://linkinghub.elsevier.com/retrieve/pii/S0272884223006259

[16] Sangeetha G, Sekhar KC, Hameed A, Ramadevudu G, Chary MN, Shareefuddin M. Influence of CaO on the structure of zinc sodium tetra borate glasses containing Cu^{2+} ions. J Non Cryst Solids. 2021;563(December 2020).

[17] Thakur V, Singh A, Punia R, Kaur M, Singh L. Effect of $BaTiO_3$ on the structural and optical properties of lithium borate glasses. Ceram Int. 2015;41(9):10957–65.

[18] Abu-khadra AS, Sadeq MS. In fl uence of Fe cations on the structural and optical properties of alkali- alkaline borate glasses. J Non Cryst Solids [Internet]. 2020;548(June):120320. Available from: https://doi.org/10.1016/j.jnoncrysol.2020.120320

Online ISSN: 3009-7800
Print ISSN: 3009-6324

[19] Supasai T, Dangtip S, Learngarunsri P, Boonyopakorn N, Wisitsoraat A, Hodak SK. Applied Surface Science Influence of temperature annealing on optical properties of $SrTiO_3$ / $BaTiO_3$ multilayered films on indium tin oxide. 2010;256:4462–7.

[20] Thakur S, Aliyu US, Singh L, Thakur V. Effect of Er3+ ions on the structural, optical and Judd-Ofelt (JO) intensity parameters of ($Bi2O_3$-$BaTiO_3$) glass system and their application as fiber-amplifier. Mater Chem Phys [Internet]. 2022 Dec;292(August):126782. Available from: https://linkinghub.elsevier.com/retrieve/pii/S0254058422010884

[21] Ramezani A, Abdizadeh H, Golobostanfard MR. Optical properties of multi-stacked $BaTiO_3$/$SrTiO_3$ thin films synthesized via chemical method. Ceram Int [Internet]. 2021 Jul;47(13):17895–906. Available from: https://linkinghub.elsevier.com/retrieve/pii/S0272884221007689

[22] Misbah MH, El-Kemary M, Ramadan R. Effect of Mg^{2+} coordination on the structural and optical properties of iron magnesium phosphate glasses. J Non Cryst Solids. 2021;569(June 2020):2043–9.

[23] Soliman TS, Zaki MF, Hessien MM, Elkalashy SI. The structure and optical properties of PVA-$BaTiO_3$ nanocomposite films. Opt Mater (Amst) [Internet]. 2021 Jan;111(October 2020):110648. Available from: https://linkinghub.elsevier.com/retrieve/pii/S0925346720309885

[24] Chuah GK, Jaenicke S, Pong BK. The preparation of high-surface-area zirconia: II. Influence of precipitating agent and digestion on the morphology and microstructure of hydrous zirconia. J Catal [Internet]. 1998 Apr;175(1):80–92. Available from: https://linkinghub.elsevier.com/retrieve/pii/S0021951798919807

[25] Kandjani AE, Sabri YM, Coyle VE, Harrison CJ, Korcoban D, Canjeevaram Balasubramanyam RK, et al. Long-range ordered TiO_2/Au hollow urchins: topology control for maskless electrodeposition. J Mater Chem A. 2020;8(48):26035–44.

[26] Yaghoubi H, Li Z, Chen Y, Ngo HT, Bhethanabotla VR, Joseph B, et al. Toward a Visible Light-Driven Photocatalyst: The Effect of Midgap-States-Induced Energy Gap of Undoped TiO_2 Nanoparticles. ACS Catal [Internet]. 2015 Jan 2;5(1):327–35. Available from: https://pubs.acs.org/doi/10.1021/cs501539q

[27] Choudhury B, Choudhury A. Oxygen defect dependent variation of band gap, Urbach energy and luminescence property of anatase, anatase-rutile mixed phase and of rutile phases of TiO_2 nanoparticles. Phys E Low-Dimensional Syst Nanostructures. 2014;56:364–71.

[28] Umar SA, S.N N, Geidam IG, El-Mallawany R, M. Abd-Elnaiem A, Hakamy A, et al. Optical basicity, polarizability and spectroscopic investigations of CuO doped TeO_2–B_2O_3 glass system. Mater Chem Phys [Internet]. 2023 Mar;297(March 2022):127309. Available from: https://linkinghub.elsevier.com/retrieve/pii/S0254058423000172

Online ISSN: 3009-7800
Print ISSN: 3009-6324

[29] Hussien SA, Saad EM, Gaber EA, Mahmoud AE razek, Morshidy HY. Impactive cadmium modifications to enhance the structural-optical relationship in nickel borate glasses. Ceram Int [Internet]. 2023 Jul;49(14):22989–3002. Available from: https://linkinghub.elsevier.com/retrieve/pii/S0272884223010787

[30] Azlina Y, Azlan MN, Hajer SS, Halimah MK, Suriani AB, Umar SA, et al. Graphene oxide deposition on neodymium doped zinc borotellurite glass surface: Optical and polarizability study for future fiber optics. Opt Mater (Amst) [Internet]. 2021 Jul;117(May):111138. Available from: https://linkinghub.elsevier.com/retrieve/pii/S0925346721003396

[31] Azlan MN, Halimah MK, Suriani AB, Azlina Y, El-Mallawany R. Electronic polarizability and third-order nonlinearity of Nd^{3+} doped borotellurite glass for potential optical fiber. Mater Chem Phys. 2019;236(May).

[32] Morshidy HY, Mohamed AR, Abul-Magd AA, Hassan MA. Role of high energy Cr^{6+} optical transition induced by rare earth ion (La^{3+}) in compositional-dependent borate glass. Mater Chem Phys. 2022;289(June).

[33] Babeer AM, Mahmoud AE razek, Morshidy HY. Ligand field parameters, optical, thermal, magnetic, and structural features of ZnO containing cobalt-borate glasses. Mater Chem Phys. 2023;302(April).

[34] Garmire E. Overview of Nonlinear Optics. In: Nonlinear Optics [Internet]. InTech; 2012. Available from: http://www.intechopen.com/books/nonlinear-optics/overview-of-nonlinear-optics

[35] Wen X, Gong Z, Li D. Nonlinear optics of two-dimensional transition metal dichalcogenides. InfoMat [Internet]. 2019 Sep 23;1(3):317–37. Available from: https://onlinelibrary.wiley.com/doi/10.1002/inf2.12024

[36] Keshavamurthy K, Swetha BN, Al–Harbi FF, G J, Almuqrin AH, Sayyed MI, et al. Improved near–infrared nonlinear optical properties of Sm^{3+} containing borate glasses: Effect of silver nanoparticles concentration. Opt Mater (Amst) [Internet]. 2021 Dec;122:111804. Available from: https://linkinghub.elsevier.com/retrieve/pii/S0925346721010041

[37] El-Metwally EG, Hegab NA, Mostfa M. Linear and non-linear optical dispersion parameters of $Te_{81}Ge_{15}Bi_4$ chalcogenide glass thin films for optoelectronic applications. Phys B Condens Matter. 2022;626(November 2021).

Online ISSN: 3009-7800
Print ISSN: 3009-6324